International Journal of Biological Macromolecules 132 (2019) 929–938

Contents lists available at ScienceDirect

International Journal of Biological Macromolecules

journal homepage: http://www.elsevier.com/locate/ijbiomac

Double-edged effects of aluminium ions on amyloid fibrillation of hen egg-white lysozyme

Lei Xing [1], Ning Chen [1], Wei Fan, Mengna Li, Xiaoguo Zhou *, Shilin Liu *

Hefei National Laboratory for Physical Sciences at the Microscale, iChEM (Collaborative Innovation Center of Chemistry for Energy Materials), Department of Chemical Physics, University of Science and Technology of China, Hefei, Anhui 230026, China

ARTICLE INFO

Article history:
Received 22 January 2019
Received in revised form 30 March 2019
Accepted 2 April 2019
Available online 04 April 2019

Keywords:
Raman spectroscopy
Kinetics
Amyloid fibrils

ABSTRACT

Elucidating the effects of Al(III) ions on amyloid fibrillation is important to understand the association between metal ions and Alzheimer's disease. Here, Raman spectroscopy was applied to investigate amyloid fibrillation of hen egg-white lysozymes during thermal incubation with Al(III) ions or acids, combined with atomic force microscopy and thioflavin T fluorescence assays. Kinetics of conformational changes in lysozymes were assessed by monitoring six characteristic Raman spectral markers. The peak of Phe residues at 1003 cm^{-1} and two bands of Trp residues at 759 cm^{-1} and 1340–1360 cm^{-1} corresponded to the lysozyme tertiary structure, whereas two N—C_α—C stretching vibrations at 899 cm^{-1} and 935 cm^{-1} and an amide I band were associated with the lysozyme skeleton. There may be a four-stage transformation mechanism underlying the kinetics of amyloid fibrillation of lysozymes with the thermal/Al(III) treatment. Comparison of kinetics under thermal/Al(III) and thermal/acid conditions revealed double-edged roles of Al(III) ions in amyloid fibrillation of lysozymes. Specifically, in addition to postponing α-helix degradation, Al(III) ions accelerated conformational transformations from α-helices to organized β-sheets. The present investigation sheds light on the controversial effects of Al(III) ions on amyloid fibrillation of lysozymes.

1. Introduction

Distinct functions of proteins in living organisms are strongly associated with their specific three-dimensional structures, which can be disrupted under certain conditions and self-assembled to form amyloid fibrils. This self-assembly can trigger many human neurodegenerative diseases, such as Alzheimer's disease (AD) and Parkinson's disease [1–3]. As a model protein, hen egg-white lysozyme (HEWL) has been widely used to study amyloid fibrillation because fibrillation of HEWL amyloids is similar to that of amyloid-β (Aβ) proteins associated with AD [4–9]. Indeed, under the action of fibrillation factors, amyloid fibrillation of lysozymes occurs after a certain incubation period [9].

Among environmental variables, temperature, pH, and metal ions are the factors associated with fibrillation [10]. In addition to effects of heat and acid treatments [11–14], influences of several metal ions, such as Zn^{2+} [15], Cu^{2+} [16,17], Fe^{3+} [18], and Mn^{2+} [19,20], on amyloid fibrillation have been investigated. Moreover, association between Al(III) ions and degenerative diseases has long been argued [21–24]. Numerous investigations have concluded that Al(III) ions are the potential etiological factor for AD [25–29] and that these ions accelerate formation of Aβ peptides and other protein fibrils. However, these conclusions have been queried recently because not all patients show high Al(III) concentrations in brain tissues [21,24,30]. Moreover, excessive Al(III) intake is more toxic to the body than to the brain, and experimental animals tend to die or become seriously ill before protein aggregation begins [31]. Thus, convictive evidence of the association between Al(III) ions and AD is still lacking.

To the best of our knowledge, mechanisms through which Al(III) ions affect amyloid fibrillation have been scarcely investigated. Uversky et al. found that Al(III) ions prominently accelerated the formation of α-synuclein fibrils [32], but Xu et al. found that Al(III)/EGCG complexes (molar ratio of 1:1) inhibited hIAPP fibrillation more efficiently than did EGCG alone [33]. Moreover, in recent AFM and ThT fluorescence assays, Al(III) ions inhibited fibrillation of hIAPP (11–28) peptides [34]. Curcumin—a JNK blocker—reportedly inhibited the promoting effects of Al(III) ions on amyloid fibrillation of β-lactoglobulin [35]. Similarly, many medicines, including ascorbic acid, capreomycin, vitamin k3, vitamin B12, and ibuprofen, have been found to inhibit protein fibrillation [36–41]. According to a theoretical calculation that was proposed to elucidate mechanisms of Al(III) toxicity in brain tissues, Al(III) ions could bind to amide nitrogen and carbonyl oxygen of the peptide backbone to form a ring structure that induced irreversible protein denaturation [42]. In summary, influence of Al(III) ions on amyloid fibrillation of lysozymes remains controversial.

* Corresponding authors.
E-mail addresses: xzhou@ustc.edu.cn (X. Zhou), slliu@ustc.edu.cn (S. Liu).
[1] These authors contributed equally to this work.

https://doi.org/10.1016/j.ijbiomac.2019.04.009
0141-8130/

Spectroscopic techniques can be used to detect transformations of structural configurations. Thus, mechanisms through which Al(III) ions act can be revealed based on conformational changes during protein fibrillation following the thermal/Al(III) treatment, and these data may be favorable for drug development. Due to its high sensitivity, Fourier transform infrared (FTIR) spectroscopy is widely used to detect secondary protein structures [43,44]. However, the H–D exchange is inevitable during analyses of IR spectra in deuterated aqueous solutions. Moreover, IR intensities of aromatic amino acid side chains are rather weak to be efficiently detected in aqueous solutions, and spectral data of these residues are critical for characterization of protein structures. Fortunately, vibrations of these side chains and skeletons exhibit visible Raman intensities in aqueous protein solutions. In particular, Raman shifts, intensities, and bandwidths are sensitive to local environments [45,46]. Hence, in contrast to FTIR spectroscopy, Raman spectroscopy can be used to identify conformations of polypeptides and proteins [47–51]. An excellent review has been published recently summarizing progress in Raman spectral investigations of amyloid fibrillation [50]. Combined with AFM and ThT fluorescence assays, Raman spectroscopy can serve as the most powerful experimental approach for investigating protein structures [47–51]. Very recently, we successfully applied a combination of these spectroscopic techniques in a study of amyloid fibrillation kinetics of HEWL under thermal and acidic conditions and proposed a four-stage transformation mechanism [52].

Herein, we investigated roles of Al(III) ions in HEWL amyloid fibrillation. Protein morphologies and conformational transformations during fibrillation were monitored using AFM and ThT fluorescence assays. Changes in secondary and tertiary structures of lysozymes in aqueous solutions during amyloid fibrillation under thermal/Al(III) and thermal/acid conditions were detected using Raman spectroscopy. The amyloid fibrillation kinetics of HEWL mediated by Al(III) ions or acids in heated aqueous solutions were analyzed based on incubation time dependencies of various Raman bands. Finally, effects of Al(III) ions on HEWL amyloid fibrillation were clarified by comparing kinetic differences in amyloid fibrillation between thermal/Al(III) and thermal/acid treatments.

2. Experimental

2.1. Solution preparation

HEWL in the native state was purchased from Sangon Biotech (Shanghai) Co. Ltd. and was used without further purification. Amyloid fibrillation of lysozymes was induced as described previously [4,7,53]. The initial lysozyme concentration was 20 mg/mL in aqueous solution. To investigate effects of Al(III) ions, $AlCl_3$ was added to heated lysozyme solutions at a concentration of 0.02 mol/L. We refer to these conditions as the thermal/Al(III) treatment. As indicated previously [32,54,55], chloride ions show very little concentration-dependent influence on protein structures. Hence, for comparison, amyloid fibrillation was monitored under thermal and acidic conditions (pH 2.0) by adding hydrochloric acid. Solutions in sealed glass vials were incubated in a thermoshaker at 65 °C without agitation. At various incubation times, aliquots of the fibril-forming solution were taken from vials, and the gelatinous phase was separated using centrifugation at 12000*g* for 20 min. Aliquots of the supernatant were directly used for Raman spectroscopy, ThT fluorescence assays, and AFM. A previous study confirmed that small amounts of fibrils remain suspended in the supernatants [8]. Thus, to verify contributors of Raman spectra in supernatants, Raman spectra of supernatant with the >200-h thermal/acid treatment and gelation after lyophilization were recorded using a confocal micro-Raman spectrometer (Fig. S1). Almost identical spectra were generated after normalization, indicating that as the dominant structure in the gelatinous phase, mature fibrils remained in supernatants after amyloid fibrillation. Therefore, the spectral features of the major products at all stages of fibrillation could be observed in Raman spectra of supernatants.

2.2. Raman spectroscopy

Raman spectroscopy was performed as described elsewhere [50,53,56]. Briefly, CW laser (Coherent, Verdi 532 nm) beam with a power of 4 W was employed as the excitation light. The confocal geometry comprised an $f = 5$ cm lens in front of the sample cell to focus excitation light and collect scattered light. Scattered light was then converged into a triple monochromator (Acton Research, TriplePro) through an $f = 20$ cm lens, and dispersed spectra were recorded using a liquid-nitrogen-cooled CCD detector (Princeton Instruments, Spec-10:100B). Sample solutions were stored in a 10 mm × 10 mm quartz cuvette at the set temperature. The resolution of Raman spectra was ~1 cm^{-1} in the region of 650–1800 cm^{-1}. Raman shifts were carefully calibrated using standard spectral lines from a mercury lamp. The acquisition time for recording spectra was approximately 1 min. Raman spectra were averaged from 20 acquisitions under the same conditions and corrected by subtracting the spectra of water with Al(III) ions measured under identical conditions. These data processes provided sufficiently reliable spectra.

2.3. Atomic Force Microscope (AFM)

All AFM images were obtained with air-dried samples under a Veeco DI-MultiMode V scanning probe microscope in the tapping mode using a 5 μm × 5 μm scanner. Protein solutions were diluted 100 times in Milli-Q water and dropped onto freshly cleaved mica. After 15 min, protein solutions were rinsed three times with deionized water. Mica surfaces were dried at room temperature, and samples were stored in a desiccator. AFM images were processed using the open-access software from Nanoscope Inc.

2.4. ThT fluorescence assays

Steady-state fluorescence emissions of the ThT dye (1×10^{-5} mol/L) were measured using a fluorescence spectrophotometer (Shimadzu, F-4600) within a wavelength range of 400–800 nm. An excitation wavelength of 420 nm was selected, and emission at 480 nm was selected to represent the fluorescence intensity. All measurements were performed under ambient conditions. During HEWL amyloid fibrillation, 40-μL aliquots of the supernatant were picked up from vials after various incubation times and were added to 960 μL ThT solutions. *Ex situ* fluorescence assays of the solutions were performed immediately. Intensities were averaged from 15 acquisitions at various incubation times.

3. Results and discussion

3.1. AFM images of lysozyme with thermal/Al(III) or thermal/acid treatments

Morphological changes in proteins during amyloid fibrillation were visible in AFM images (Fig. 1) obtained at various incubation times. During the very early stage of aggregation (Fig. 1a), no changes were observed because the proteins in the native state were too small. Subsequently, however, spheroidal aggregates became visible, which comprised oligomers (Fig. 1b). Under the thermal/Al(III) conditions, lysozyme fibrils were clearly formed after incubation for 196 h (Fig. 1c). These fibrils aggregated to form mature fibrils with average heights of 6–10 nm and lengths of a few microns. Morphologies of lysozyme fibrils formed under thermal and acidic conditions are shown in Fig. 1d. Obviously, the morphologies with the two treatments were similar despite slightly different formation rates. However, when thermally incubated without Al(III) ions or acids, only a few spheroidal aggregates were formed after 30 h and no fibrils were produced even after >200 h (Fig. 1e and f). These results demonstrated that Al(III) ions and acids efficiently promoted lysozyme fibril formation.

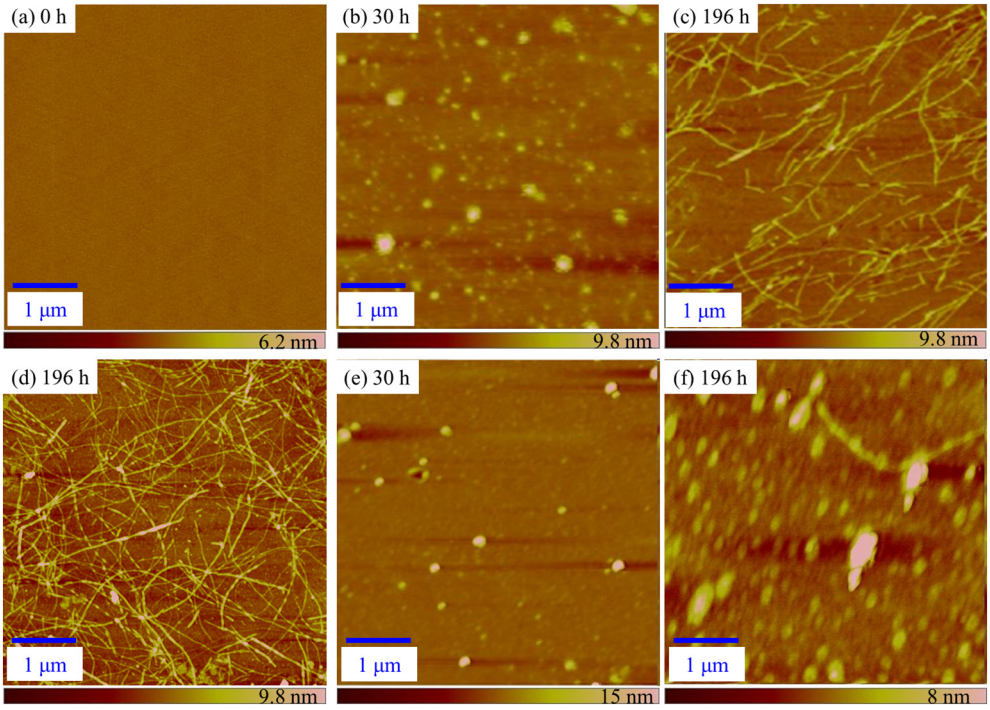

Fig. 1. AFM height images of lysozyme with the thermal/Al(III) treatment at various incubation periods: (a) initial native state; (b) oligomers produced after 30-h incubation period; (c) fibrils formed after 196-h incubation period. AFM images of mature fibrils formed under thermal and acidic conditions are shown (d). For comparison, AFM images of lysozyme incubated at 65 °C in the absence of Al(III) ions or acids after (e) 30 h and (f) 196 h are shown. No dilution was performed due to insufficient quantities of oligomers.

3.2. ThT fluorescence spectra of lysozyme

When ThT is added to protein solutions, its fluorescence intensity at ~480 nm may be enhanced by amyloid fibrillation [43,57]. Surfaces of the protein cross-β structures form ThT-binding sites, where the surface-exposed grooves lined with aromatic amino acids of side chains form extended channel-like motifs. Accordingly, free rotations of bound benzylamine and benzathiole rings of ThT are restricted in these channels, enhancing fluorescence intensities [58]. Therefore, ThT fluorescence is widely used as the gold standard for selective staining and quantification of the formation of cross β-sheet-rich structures during amyloid fibrillation.

Fig. 2 shows fluorescence spectra of lysozymes in the native state and mature fibrils in aqueous solutions with thermal/Al(III) and thermal/acidic treatments. Fluorescence spectra of soluble aggregates formed during thermal incubation in the absence of Al(III) ions and acids are also shown. Compared with those of the native lysozyme, fluorescence intensities of aggregates (in blue) and fibrils (in green) were

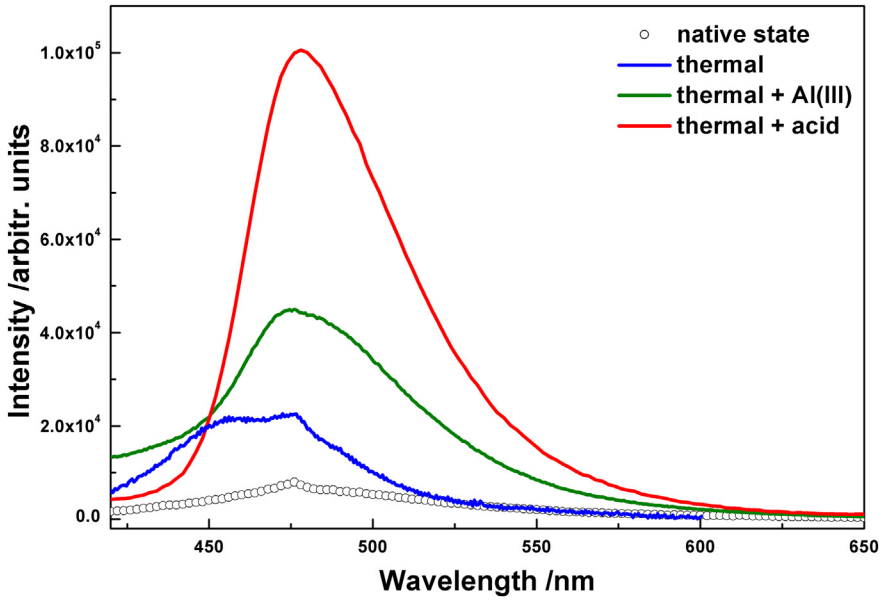

Fig. 2. ThT fluorescence spectra of the native lysozyme (in black circles) and fibrils (in solid traces) with thermal/Al(III) (in green) and thermal/acid (in red) treatments. Blue curve represents the spectra of soluble aggregates formed during thermal incubation in the absence of Al(III) ions or acids. (For interpretation of the references to color in this figure legend, the reader is referred to the web version of this article.)

enhanced by approximately 2.8-fold and 5.6-fold, respectively. In contrast, fluorescence intensities of fibrils formed in heated and acidic solutions (in red) were dramatically increased by >12-fold. These observations suggest that Al(III) ions are weaker inducers of protein fibril formation than acids, as observed in a previous study of fibrillation using hIAPP (11-28) peptides [34]. Other recent investigations showed that due to electrostatic repulsions, highly positive charged fibrils did not appreciably bind with ThT [59,60]. Therefore, fibrils show reduced ThT-binding capacity after binding with Al(III) ions, leading to naturally reduced fluorescence intensities.

In addition, an unexpected shoulder peak was observed at ~455 nm in the spectrum of soluble aggregates formed in thermally incubated solutions without Al(III) ions or acids. In the absence of repulsive electrostatic interactions, ThT preferentially binds to a minimal groove formed by four aromatic–hydrophobic cross-strand residues [61]. However, suitable ThT-binding motifs are not present in twisted β-sheets comprising fewer than four β-strands, such as those of typical globular proteins [62,63]. Therefore, during thermal incubation in the absence of Al(III) ions and acids, more disordered β-sheet structures were formed in the aggregates, although their sizes appeared similar to the organized aggregates observed in AFM images.

Finally, we recorded the kinetics of ThT fluorescence over time as a typical sigmoid functional relationship, and we compared these data with Raman analyses data in Section 3.4.

3.3. Raman spectra of the native lysozyme and mature fibrils

Raman spectroscopy is a powerful technique for detecting changes in protein molecular structures [47–51]. We investigated lysozyme aggregation under thermal/Al(III) and thermal/acid conditions using Raman spectroscopy and observed the kinetics of this process *in situ*. Fig. 3 shows the Raman spectra of the native lysozyme and formed mature fibrils. Typical raw data are shown in Fig. S2. Because protein concentrations in the supernatants were reduced following fibril formation and gelation, intensities of all vibrational peaks were weaker than those of the native lysozyme. As suggested previously [64–66], spectral intensity of the Phe ring was insensitive to the microenvironment and reflected protein concentrations. Hence, the Phe band at 1003 cm^{-1} was used to normalize the band intensities shown in Fig. 3.

Multiple vibrational peaks were observed in the spectra shown in Fig. 3, and some of these were unassigned until date. Only six well-known bands were used to qualitatively and quantitatively assess structural changes during amyloid fibrillation. As listed in Table 1, these changes were classified into vibrational bands of skeletons and side groups of lysozyme. The two N—C_α—C stretching vibrations and the amide I band were selected to indicate conformational transformations of the lysozyme skeleton, whereas the vibrational peaks contributed by Trp and Phe residues were used to monitor changes in side chain microenvironments.

No changes in spectra were apparent during thermal incubation in the absence of Al(III) ions and acids, indicating stability of the lysozyme structure (Fig. S3). In the absence of acids or Al(III) ions, unfolding of tertiary structures occurred very slowly, leading to insufficient proportions of soluble aggregates in the solution. Accordingly, oligomer concentrations were limited in AFM images of undiluted solutions (Fig. 1e and f). In the presence of Al(III) ions or acids, however, remarkable changes in fibril spectra were observed (Fig. 3b), including Raman shifts of the bands at ~899 cm^{-1}, ~935 cm^{-1}, and ~1658 cm^{-1}. In addition, the spectra of mature fibrils formed under the two conditions (red and blue traces) were almost identical, indicating that Al(III) ions did not affect mature fibril structures. These observations were confirmed in AFM images.

Raman bands of aromatic amino acid side chains, such as those at ~759 cm^{-1}, ~1003 cm^{-1}, and ~1350 cm^{-1}, are often used to monitor tertiary structures of proteins. In particular, the peak at ~759 cm^{-1} was attributed to coupled vibrations of the in-phase symmetric ring breathing of benzene and pyrrole rings of Trp [67,68], and its intensity was very sensitive to distortions of the indole ring under differing local environments. FWHM increased from 8.3 cm^{-1} in the native state to 9.7 cm^{-1} in fibrils, indicating wider conformational distributions of Trp in lysozyme fibrils (Fig. 4a) [45]. Moreover, double peaks at 1340 cm^{-1} and 1360 cm^{-1} represent Fermi resonances of Trp and comprise a fundamental in-plane C_8═N_1 stretching and a combination of out-of-plane deformations of indole rings [45,67,68]. The intensity ratio of this doublet, I_{1340}/I_{1360}, was also sensitive to the degree of Trp hydration [69]. When I_{1340}/I_{1360} is >1.0, the indole ring of Trp is exposed to the aqueous medium or is in contact with aliphatic side chains. Conversely, the surrounding hydrophobic residues are expected to be located close to the indole ring of Trp [68,69]. The I_{1340}/I_{1360} ratio visibly

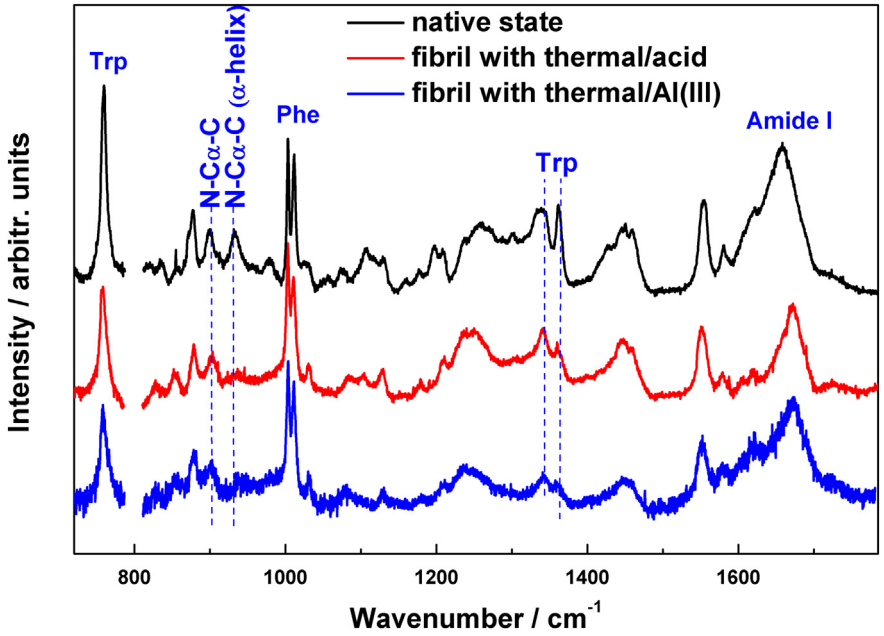

Fig. 3. Raman spectra of the native lysozyme (in black) and fibrils formed with the thermal/Al(III) (in blue) and thermal/acid (in red) treatments. Major characteristic vibrational bands are marked and represent protein structure changes. (For interpretation of the references to color in this figure legend, the reader is referred to the web version of this article.)

Table 1
Assignments and spectral features of the specific Raman bands of lysozyme.

Molecular groups	Raman-shift/cm^{-1}[a]	Assignment	Raman markers[b]
Trp	759(759)	coupled vibrations of in-phase breathings of benzene and pyrrole	FWHM [70,85]
N-C_α-C	899(904)	N—C_α—C stretching	Peak position [45,67,68,70,86]
	932(939)	stretching of N—C_α—C segment in α-helical structures	Peak position [45,67,68,70,86]
Phe	1003(1003)	ring breathing of benzene in Phe amino residue	FWHM [67,68]
Trp	1340/1360 (1340/1360)	Fermi resonances between the fundamental in-plane N_1=C_8 stretching and the combination bands of ring out of plane deformations.	I_{1340}/I_{1360} [45,68]
Amide	1658(1671)	"Amide I" as the coupling mode of the C=O and C—N stretching vibration and a small amount of N—H in-plane bending vibration	Peak position [67,87]

[a] The values in parentheses are the corresponding Raman shifts of the mature fibrils.
[b] FWHM is the full-width at half maximum.

increased after amyloid formation, indicating that the local environments around Trp side chains became more hydrophilic with conformational changes from the native state to fibrils (Fig. 4c).

The band at 1003 cm^{-1} was assigned to benzene ring breathing in Phe residues [67,68]. Similar to the Trp peak at 759 cm^{-1}, FWHM at 1003 cm^{-1} (Fig. 4b) expanded with the loosening of tertiary protein structures, leading to the exposure of Phe residues [8]. During partial unfolding, various rotational isomers with different vibrational frequencies are formed from the initial rigid configurations of lysozymes [70]. Consequently, these Raman resonances broaden and weaken.

The most commonly used Raman fingerprints of lysozyme skeleton structures comprise the bands at 899 cm^{-1}, 935 cm^{-1}, and 1650 cm^{-1}. The first two bands are attributed to the N—C_α—C stretching vibrations of skeletons, and the 935-cm^{-1} band is

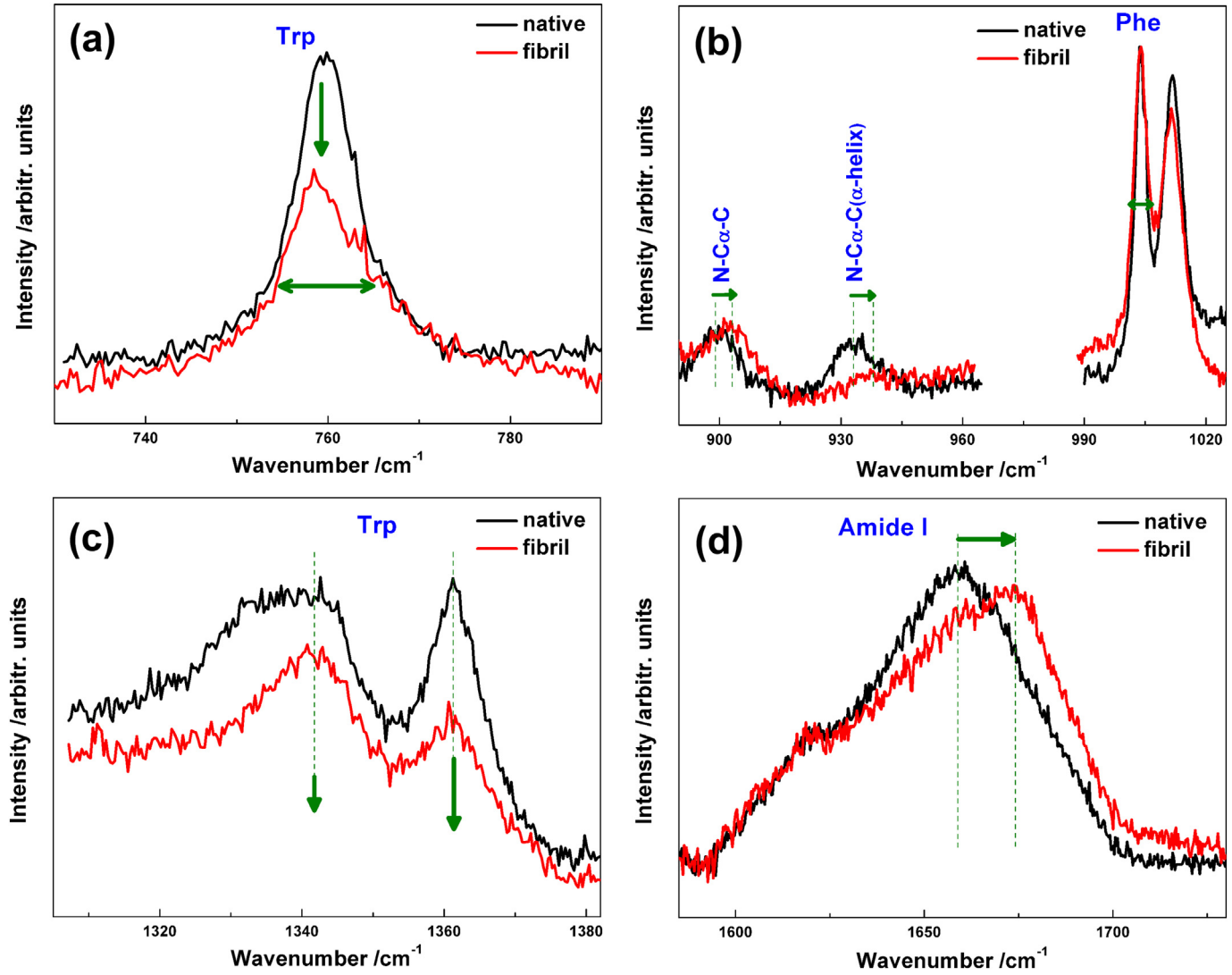

Fig. 4. Magnified Raman spectra of lysozyme in the native state (in black) and mature fibrils (in red) with the thermal/Al(III) treatment: (a) 730–790 cm^{-1}, (b) 890–1025 cm^{-1}, (c) 1305–1382 cm^{-1}, (d) 1585–1730 cm^{-1}. (For interpretation of the references to color in this figure legend, the reader is referred to the web version of this article.)

predominantly associated with α-helical secondary structures [45]. Both these bands are highly sensitive to conformations of N—$C_α$—C segments [45]. In magnified spectra shown in Fig. 4b, a blue shift of the N—$C_α$—C peak at 899 cm^{-1} is apparent, indicating conformational transformation of the N—$C_α$—C skeleton. Moreover, the intensity of the band at 935 cm^{-1} dramatically decreased upon lysozyme denaturation from the native state to fibrils, indicating the loss of α-helical structures. These data are in general agreement with previous reports [7,8,71].

The peak at ~1650 cm^{-1} is well known as an amide I vibration that covers the range of 1640–1680 cm^{-1}. This vibration mostly comprises the C═O stretching, C—N stretching, and N—H in-plane bending vibrations of amino acid residues [72]. Multiple previous studies have shown specific resonance frequencies of vibration in differing secondary protein structures [67,68,73,74]. These frequencies reflect relative strengths of hydrogen bonding interactions (C═O···H) between amide groups and dipole–dipole interactions between carboxyl groups. In lysozyme, α-helical structures usually have low-frequency accordion-like motions that contribute to intensities of bands at 1640–1660 cm^{-1} [67,74], and organized β-sheets contribute the bands at 1660–1680 cm^{-1} [7,75,76]. In contrast, frequencies of disordered structures (random coils), such as β-turns, loose β-strands, and polyproline structures, are lower than 1640 cm^{-1} or higher than 1680 cm^{-1} [45,67]. Therefore, the present amide I band can be used as an additional sensitive spectral probe for protein skeleton structures.

The amide I peak position of mature fibrils exhibits a blue shift of 10 cm^{-1} from that in the native state, indicating transformation of the α-helical secondary structures of lysozyme to other conformations, such as β-sheets or random coils, during amyloid fibrillation (Fig. 4d). Moreover, organized β-sheets were the dominant secondary structure in mature fibrils.

3.4. Time-dependence curves under the thermal/Al(III) conditions

To precisely investigate the kinetics of lysozymes during amyloid fibrillation, we monitored secondary and tertiary structure changes over time using corresponding Raman markers. Fig. 5 shows changes in Raman spectral features of Trp and Phe residues under the thermal/Al(III) conditions. These curves clearly exhibit a two-stage feature that differs from single exponential growth relationships of these markers under thermal/acid conditions (Fig. S4). Initially, FWHM and I_{1340}/I_{1360} ratios of Trp as well as FWHM of the Phe band at 1003 cm^{-1} increased monotonically, indicating exposure of more side chain Trp or Phe residues to hydrophilic environments following partial unfolding of tertiary structures. The corresponding conformational distributions also became wider. After incubation for ~10 h, variations of the three markers were slower, but rapid growth was resumed at ~40 h. All spectral indicators reached their maximums ~120 h later. Additionally, we observed a similar two-stage change in the transmittance of solutions. After ~10-h incubation, transmittance began to decrease due to the formation of spheroidal oligomers, as indicated by corresponding AFM images. During the period from 25 to 40 h, however, transmittance changed very slowly, suggesting a kinetic equilibrium between the formation and degradation of oligomers [77]. Subsequently, degradation gradually dominated with transformation of secondary structures after incubation for ~40 h, and the degraded oligomers assembled into amyloidogenic protofibrils or amorphous gels. Hence, transmittance was further reduced until ~80 h.

Differing kinetic behaviors were observed among the Raman markers for lysozyme skeleton structures (Fig. 6). All curves exhibited typical one-stage changes, in which protein aggregation endured a lag phase, followed by a rapid growth phase and an equilibrium phase [78,79]. As described previously [80–82], we fitted a sigmoid functional relationship to the incubation time-dependent curve using eq. (1):

$$P = P_D + \frac{P_N - P_D}{1 + \exp[(T - T_m)/\Delta T]} \quad (1)$$

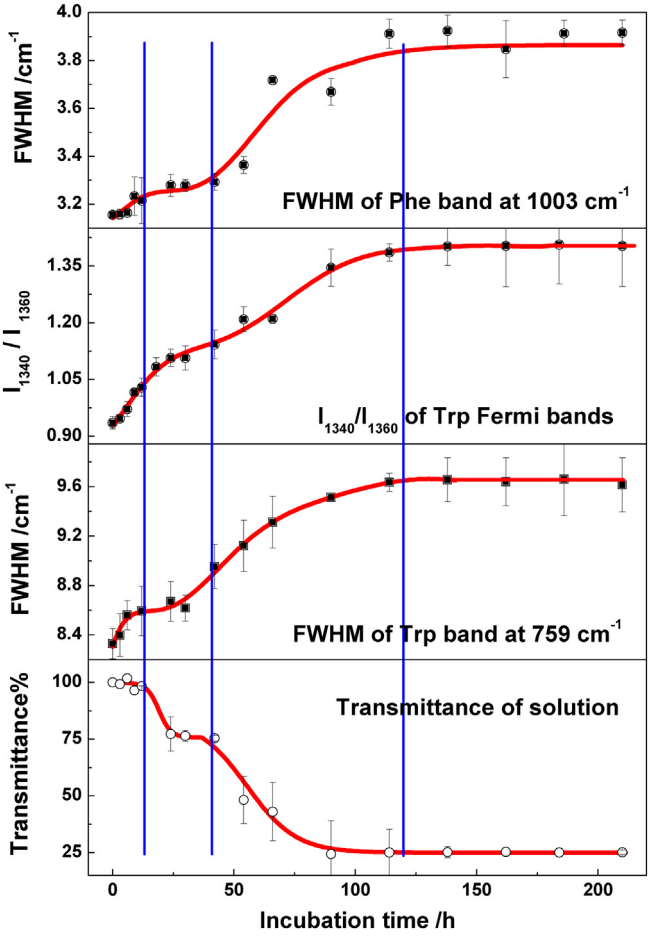

Fig. 5. Time-dependence curves of Trp and Phe residues in side chains of lysozyme and transmittance of the solution during thermal incubation with Al(III) ions.

where P_N and P_D are spectral parameters (peak position or intensity) of the initial and final states, respectively; T_m is the midpoint transition time; and 2 × ΔT corresponds with the transition time interval.

The lag durations of both spectral markers for N—$C_α$—C segments were approximately 40 h, and corresponding growth phases were not saturated until 120 h. The peak position of the amide I band changed similarly, with the lag phase lasting for ~40 h but the growth stage terminating at ~160 h (later than the growth phase of the N—$C_α$—C indicators). These almost identical lag durations of the skeleton markers indicate simultaneous uncoiling of α-helices and formation of β-sheets. Moreover, the slightly slower growth of the amide I marker indicates sequential conformational transformation of protein secondary structures.

Table 2 summarizes the midpoint transition times of the Raman markers for lysozymes during amyloid fibrillation with the thermal/Al(III) treatment. T_m values of the N—$C_α$—C marker at 899 cm^{-1} and the amide I indicator were close to each other. However, due to dramatically reduced intensities of the N—$C_α$—C band at 935 cm^{-1}, the peak position became indistinct (Fig. 4b). Thus, uncertainty of the corresponding T_m value remains for this spectral indicator. For comparison, we present previous measurements of fibrillation under thermal and acidic conditions (65 °C and pH 2.0) along with the corresponding kinetic curves (Fig. S5). T_m values of the four Raman markers under the thermal/acid conditions were lower than the corresponding values with the thermal/Al(III) treatment. Hence, acids are more efficient denaturants for amyloid fibrillation of lysozymes. Moreover, T_m values of ThT fluorescence intensities differed tremendously between treatment

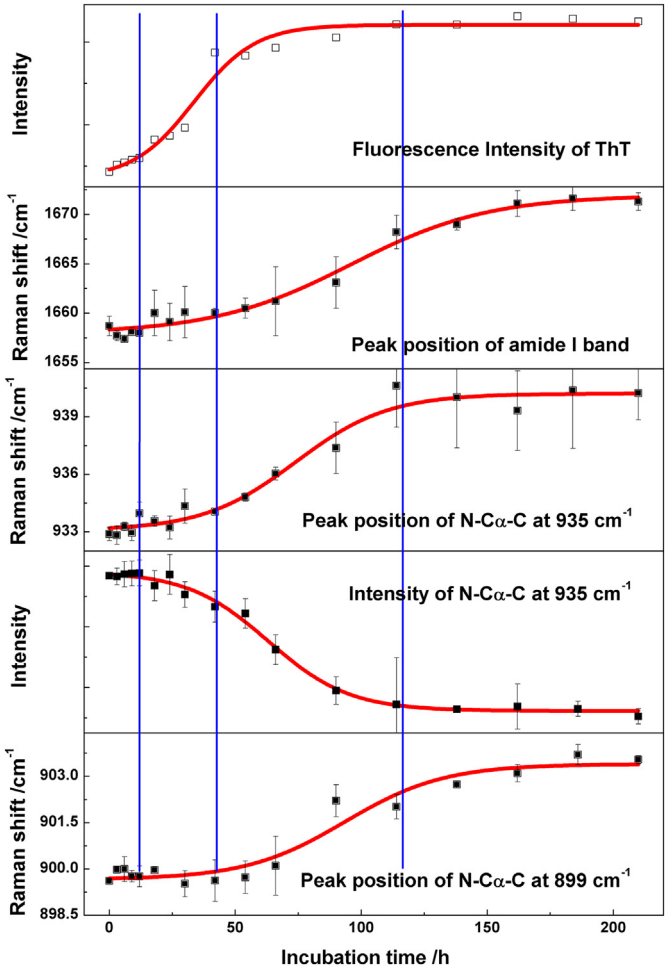

Fig. 6. Time-dependence curves of the N—C_α—C and amide I band features and ThT fluorescence intensities during thermal incubation with Al(III) ions.

conditions and were ~34 h for the thermal/Al(III) treatment and ~119 h for the thermal/acid treatment. We discuss this discrepancy in Section 3.6.

ThT fluorescence intensities during thermal incubation with Al(III) ions followed a sigmoid functional profile (Fig. 6). Specifically, ThT fluorescence rapidly increased from ~10 h due to oligomer formation. Subsequently, growth rates indicated that ThT fluorescence intensities slowed by ~40 h and approached saturation at ~80 h. These characteristic times agree precisely with the formation and degradation of oligomers (Fig. 5) but differ remarkably from times observed under thermal and acidic conditions (Fig. S5). We discuss these differences in the following section.

Table 2
The midpoint transition times (T_m) of various skeleton conformational markers during amyloid fibrillation of lysozyme with thermal/Al(III) treatment, as well as the data obtained under the heat and acidic conditions.

Raman makers	T_m/h	T_m[a]/h
Peak position of the N—C_α—C stretching at 899 cm^{-1}	93 ± 7	26 ± 12
Peak position of the N—C_α—C stretching at 935 cm^{-1}	74 ± 5	–
Intensity of the N—C_α—C stretching at 935 cm^{-1}	63 ± 2	22 ± 7
Peak position of the amide I band at ~1650 cm^{-1}	96 ± 5	59 ± 12
ThT fluorescence intensity	34 ± 3	119 ± 31

[a] From reference [44].

3.5. Four-stage mechanism of HEWL amyloid fibrillation under the thermal/Al(III) conditions

Based on the above kinetics data, we propose a four-stage mechanism of HEWL amyloid fibrillation under thermal incubation with Al(III) ions, as shown in Scheme 1.

During the initial stage of incubation at 65 °C (0−10 h), the convolutional three-dimensional structures of the native lysozyme unfold. As shown in Figs. 5 and 6, side chain Trp and Phe residues are gradually exposed to hydrophilic microenvironments, but the secondary protein structures remain unchanged. Consistently, molten globular intermediates were previously formed with the loss of tertiary structures but with intact secondary structures [83].

After the molten globular intermediate stage, spheroidal oligomers form gradually and can be observed in AFM images. Moreover, under the action of Al(III) ions, gelation becomes predominant and gelatinous aggregates form from the oligomers. Consequently, the transmittance of the solutions decreases gradually and subsequently remains constant as the formation and degradation of oligomers reach kinetic equilibrium. Notably, ThT fluorescence intensities were enhanced with the formation of oligomers. In the present experiments, ThT concentrations were slightly higher than the corresponding critical micellar concentration (~4×10^{-6} mol/L) [84], leading to preferential formation of ThT micelles. Moreover, oligomer structures were compact, and free rotations of the benzylamine and benzathiole rings of ThT were further restricted upon binding to aromatic side chains, such as those of Trp and Phe, leading to increased fluorescence intensities of ThT micelles. In addition, neither secondary nor tertiary protein structures exhibited changes during this period (Figs. 5 and 6).

During the third stage (~40 h), the secondary structure of lysozyme starts to transform. Specifically, populations of α-helical structures are reduced and organized β-sheets are simultaneously formed, as indicated in our time-dependent curves for the N—C_α—C and amide I bands (Fig. 6). During this period, tertiary structures continue to unfold and more gels are formed, leading to rapid minimization of solution transmittance. Subsequently, unbranched protofibrils form gradually with the transformation of secondary structures. After ~120 h, populations of protofibrils with organized β-sheets become saturated, and protofibril morphologies can be clearly observed in AFM images.

During the fourth stage (>120 h), protofibrils slowly aggregate into mature fibrils, and cross β-sheets are increasingly formed. In contrast with ThT fluorescence changes under thermal and acidic conditions, no notable enhancements of ThT fluorescence intensities were observed during this stage. As mentioned above, ThT-binding sites are located at the surfaces of cross-β structures, particularly at channel-like motifs that comprise surface-exposed grooves lined with aromatic side chain amino acids. Accordingly, ThT fluorescence was remarkably enhanced as the number of organized β-sheets increased. The contradiction between our experimental results and predictions indicates that fibrils formed under thermal/Al(III) conditions lack suitable structures for binding with ThT micelles. Indeed, corresponding AFM images showed slightly stiffer morphologies of mature fibrils formed under thermal/Al(III) conditions than those of mature fibrils formed under thermal/acidic conditions (Fig. 1d). Perhaps, the organized β-sheets in fibrils formed under the action of the Al(III) ions are narrower than four β-strands in width, precluding ThT binding. Moreover, strong positive charges of fibrils with Al(III) ions likely reduced the affinity to ThT.

3.6. Comparison of thermal/Al(III) and thermal/acid treatments

Although both acid and Al(III) treatments induce amyloid fibrillation of lysozymes, few studies have compared the ensuing differences and similarities. Previous reports only suggest that lysozymes prefer to form fibers under thermal and acidic conditions [4,8,53,75]. Although similar spectra for lysozyme fibrils were observed following thermal/Al(III) and thermal/acid treatments, time curves for spectral markers

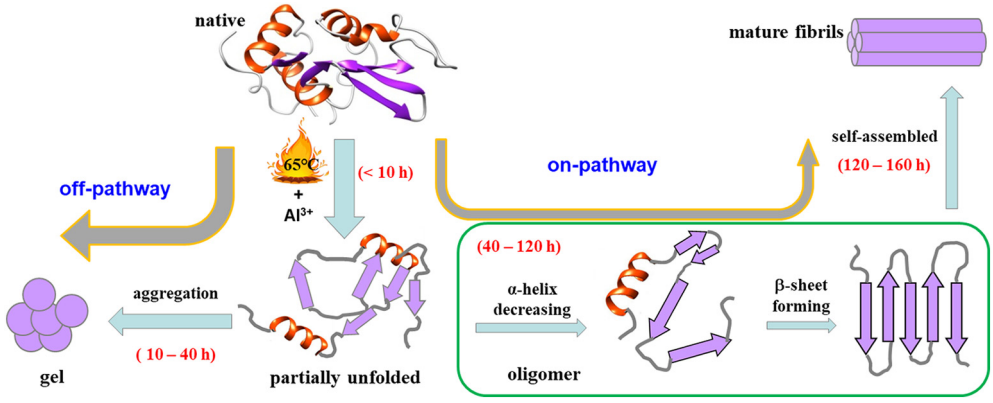

Scheme 1. Four-stage mechanism of amyloid fibrillation of lysozyme under thermal/Al(III) conditions.

differed between these two conditions. Fig. 7 shows typical curves for FWHM of the Trp band at 759 cm^{-1}, the Raman shift of the N—C_α—C stretch at 899 cm^{-1}, and the peak position of the amide I vibration.

As shown in Fig. 7a, FWHM of the Trp band at 759 cm^{-1} increased at the same rate as that during the initial stage under the action of Al(III) ions or acids. Although molten globular intermediates were formed under these conditions, growth rates decreased after 10 h in the presence of Al(III) ions [83]. These data likely reflect a sustained kinetic equilibrium between degradation and assembly of molten globular intermediates under these conditions, thus delaying the exposure of Trp residues to hydrophilic environments. In contrast, rapid growth of Trp FWHM resumed at ~40 h and reached saturation at ~120 h, clearly later than the corresponding kinetic stage in the presence of acids. Moreover, final FWHM of the band was slightly smaller in the presence of Al(III) ions than in the presence of acids, implying that the configurations of Trp amino residues are limited to some extent by bound Al(III) ions.

In contrast to observations under thermal and acidic conditions, Al(III) ions delayed peak position changes of the N—C_α—C stretching and amide I bands (Fig. 7b and c). Collectively, the spectral evidence indicates that acids accelerate amyloid fibrillation of lysozyme more efficiently than Al(III) ions. Surprisingly, however, growth phases of the two markers in Fig. 7 started almost simultaneously (at ~40 h) in the presence of Al(III) ions, precisely coinciding with the beginning of the second growth phase of the Trp indicator (Fig. 7a).

Uncoiling of α-helices and formation of organized β-sheets occurred almost simultaneously under the thermal/Al(III) conditions. In contrast, time delays are well-known for conformational transformations from α-helices to β-sheets under thermal and acidic conditions (Fig. S5). Moreover, under thermal and acidic conditions, random coils are initially formed with the destruction of α-helices and thermal diffusion mediates the gradual formation of hydrogen bond networks of the organized β-sheets between backbone N—H groups of one strand and backbone C═O groups of the adjacent strands. However, Al(III) ions bind to carbonyl oxygen atoms of peptide backbones in heated solutions [42], partially stabilizing the α-helical structures; therefore, destruction of α-helices is delayed, and ionic electrostatic forces concomitantly attract N—H groups in the backbones of the surrounding peptide strands, thus accelerating the formation of hydrogen bond networks of β-sheets. Specifically, Al(III) ions induce direct transformation of α-helices to organized β-sheets without forming intermediary random coils, resulting in simultaneous degradation of α-helices and formation of organized β-sheets.

4. Conclusions

Elucidating the role of Al(III) ions in amyloid fibrillation is important to understand the association between Al(III) ions and AD. In the present study, we employed Raman spectroscopy combined with AFM and ThT fluorescence assays to investigate the amyloid fibrillation of lysozyme under thermal/Al(III) and thermal/acid conditions.

Using well-known Raman spectral markers for tertiary and secondary protein structures, we directly assessed the time-dependent kinetics of amyloid fibrillation of lysozymes. By combining these data with morphological data of lysozyme obtained through AFM and ThT fluorescence assays, we proposed the following four-stage transformation mechanism of amyloid fibrillation of lysozyme during thermal incubation in the presence of Al(III) ions: (i) unfolding of the tertiary structure to expose aromatic side chain amino acids to water, accompanied by formation of molten globular intermediates; (ii) formation of spheroidal oligomers through degradation and assembly of globular intermediates; (iii) synchronous uncoiling of α-helical structures and formation of organized β-sheet structures; and (iv) aggregation of protofibrils to form mature fibrils.

Furthermore, the specific roles of Al(III) ions during amyloid fibrillation of lysozyme were revealed by comparing the kinetics under

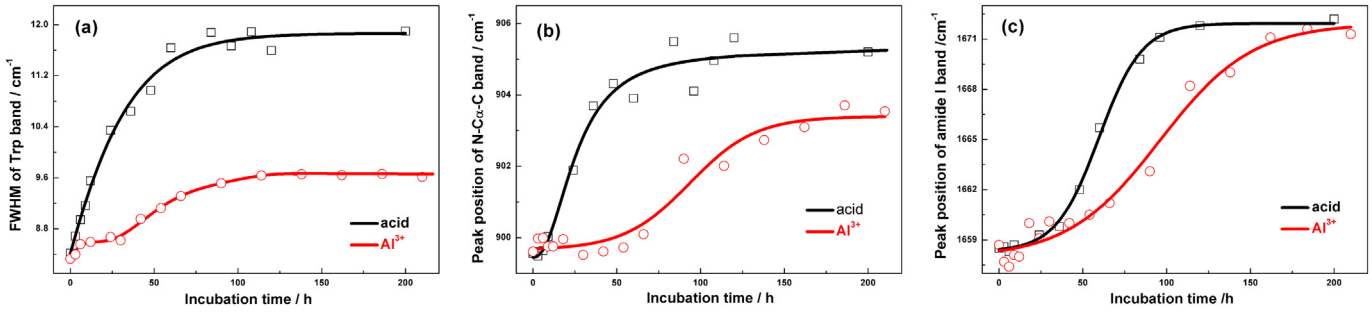

Fig. 7. Time-dependence curves of the Raman markers during amyloid fibrillation of lysozyme under thermal/Al(III) (in red) and thermal/acid (in black) conditions: (a) FWHM of the Trp band at 759 cm^{-1}, (b) Raman shift of the N—C_α—C stretching at 899 cm^{-1}, (c) peak position of the amide I vibration. (For interpretation of the references to color in this figure legend, the reader is referred to the web version of this article.)

thermal/Al(III) and thermal/acid conditions as well as under thermal incubation alone. The present spectral and ThT fluorescence data showed that Al(III) ions accelerate amyloid fibrillation of lysozyme, albeit with weaker efficacy than acids. Interestingly, a double-edged role of Al(III) ions during different stages of amyloid fibrillation was proposed. Specifically, in contrast with acid, Al(III) ions act as a stabilizer and postpone the destruction of α-helical structures of lysozyme. Nevertheless, the ionic electrostatic forces accelerate the formation of hydrogen bond networks of organized β-sheets. In another words, Al(III) ions ultimately promote the transformation from α-helices to β-sheets directly, skipping the formation of intermediate random coils.

Of note, interpretations of the data herein are subject to high concentrations of Al(III) ions required to perform experiments over reasonable periods. Nonetheless, under the present conditions, we calculated the typical inflection time points of the lag, growth, and equilibrium phases during amyloid fibrillation of lysozyme. These observations are critical to understand the entire kinetic process of amyloid fibrillation of lysozyme and may provide some clues for AD treatment. For instance, more insoluble gels were formed in heated solutions in the presence of Al(III) ions. Because toxicity of insoluble gels differs from that of amyloid fibrils, promoting or inhibiting the formation of insoluble gels may form the basis for novel treatment strategies for AD patients, as shown with the agent (−)epigallocatechin gallate [33]. Unfortunately, effects of Al(III) ions on the formation of the gelatinous phase remain unclear due to lack of data regarding oligomer structure at the molecular level. Further comprehensive spectral investigations are underway to bridge this knowledge gap.

Acknowledgments

This work was supported by the National Natural Science Foundation of China (Grant Nos. 21573208, 21573210, and 21873089) and the National Key Basic Research Foundation of China (Grant No. 2013CB834602).

Conflicts of interest

None.

Appendix A. Supplementary data

Supplementary data to this article can be found online at https://doi.org/10.1016/j.ijbiomac.2019.04.009.

References

[1] F. Chiti, C.M. Dobson, Protein misfolding, amyloid formation, and human disease: a summary of progress over the last decade, Annu. Rev. Biochem. 86 (2017) 27–68.
[2] A.S. DeToma, S. Salamekh, A. Ramamoorthy, M.H. Lim, Misfolded proteins in Alzheimer's disease and type II diabetes, Chem. Soc. Rev. 41 (2) (2012) 608–621.
[3] P. Alam, K. Siddiqi, S.K. Chturvedi, R.H. Khan, Protein aggregation: from background to inhibition strategies, Int. J. Biol. Macromol. 103 (2017) 208–219.
[4] R. Swaminathan, V.K. Ravi, S. Kumar, M.V.S. Kumar, N. Chandra, Lysozyme: a model protein for amyloid research, Adv. Protein Chem. Struct. Biol. 84 (1) (2011) 63–111.
[5] L.N. Arnaudov, R. de Vries, Thermally induced fibrillar aggregation of hen egg white lysozyme, Biophys. J. 88 (1) (2005) 515–526.
[6] S.E. Hill, J. Robinson, G. Matthews, M. Muschol, Amyloid protofibrils of lysozyme nucleate and grow via oligomer fusion, Biophys. J. 96 (9) (2009) 3781–3790.
[7] V.A. Shashilov, I.K. Lednev, 2D correlation deep UV resonance Raman spectroscopy of early events of lysozyme fibrillation: kinetic mechanism and potential interpretation pitfalls, J. Am. Chem. Soc. 130 (1) (2008) 309–317.
[8] M. Xu, V.V. Ermolenkov, W. He, V.N. Uversky, L. Fredriksen, I.K. Lednev, Lysozyme fibrillation: deep UV Raman spectroscopic characterization of protein structural transformation, Biopolymers 79 (1) (2005) 58–61.
[9] S.Y. Ow, D.E. Dunstan, The effect of concentration, temperature and stirring on hen egg white lysozyme amyloid formation, Soft Matter 9 (40) (2013) 9692–9701.
[10] W. Wang, S. Nema, D. Teagarden, Protein aggregation—pathways and influencing factors, Int. J. Pharm. 390 (2) (2010) 89–99.
[11] P. Faller, C. Hureau, O. Berthoumieu, Role of metal ions in the self-assembly of the Alzheimer's amyloid-β peptide, Inorg. Chem. 52 (21) (2013) 12193–12206.
[12] S. Bolognin, L. Messori, P. Zatta, Metal ion physiopathology in neurodegenerative disorders, NeuroMolecular Med. 11 (4) (2009) 223–238.
[13] C. Ha, J. Ryu, C.B. Park, Metal ions differentially influence the aggregation and deposition of Alzheimer's β-amyloid on a solid template, Biochemistry 46 (20) (2007) 6118–6125.
[14] I. Shcherbatykh, D.O. Carpenter, The role of metals in the etiology of Alzheimer's disease, J. Alzheimers Dis. 11 (2) (2007) 191–205.
[15] B. Ma, F. Zhang, X. Wang, X. Zhu, Investigating the inhibitory effects of zinc ions on amyloid fibril formation of hen egg-white lysozyme, Int. J. Biol. Macromol. 98 (2017) 717–722.
[16] S. Ghosh, N.K. Pandey, S. Bhattacharya, A. Roy, S. Dasgupta, Fibrillation of hen egg white lysozyme triggers reduction of copper (II), Int. J. Biol. Macromol. 51 (2012) 1–6.
[17] S. Ghosh, N.K. Pandey, S. Bhattacharya, A. Roy, N.V. Nagy, S. Dasgupta, Evidence of two oxidation states of copper during aggregation of hen egg white lysozyme (HEWL), Int. J. Biol. Macromol. 76 (2015) 1–9.
[18] E. House, J. Collingwood, A. Khan, O. Korchazkina, G. Berthon, C. Exley, Aluminium, iron, zinc and copper influence the in vitro formation of amyloid fibrils of Aβ-42 in a manner which may have consequences for metal chelation therapy in Alzheimer's disease, J. Alzheimers Dis. 6 (3) (2004) 291–301.
[19] A.B. Bowman, G.F. Kwakye, E.H. Hernandez, M. Aschner, Role of manganese in neurodegenerative diseases, J. Trace Elem. Med. Bio. 25 (4) (2011) 191–203.
[20] G.F. Kwakye, M.M.B. Paoliello, S. Mukhopadhyay, A.B. Bowman, M. Aschner, Manganese-induced Parkinsonism and Parkinson's disease: shared and distinguishable features, Int. J. Env. Res. Public Health 12 (7) (2015) 7519–7540.
[21] V.B. Gupta, S. Anitha, M. Hegde, L. Zecca, R. Garruto, R. Ravid, S. Shankar, R. Stein, P. Shanmugavelu, K.J. Rao, Aluminium in Alzheimer's disease: are we still at a crossroad? Cell. Mol. Life Sci. 62 (2) (2005) 143–158.
[22] M. Kawahara, Effects of aluminum on the nervous system and its possible link with neurodegenerative diseases, J. Alzheimers Dis. 8 (2) (2005) 171–182.
[23] M. Kawahara, M. Kato-Negishi, Link between aluminum and the pathogenesis of Alzheimer's disease: the integration of the aluminum and amyloid cascade hypotheses, Internat, Int. J. Alzheimers Dis. (2011)https://doi.org/10.4061/2011/276393.
[24] L. Tomljenovic, Aluminum and Alzheimer's disease: after a century of controversy, is there a plausible link? J. Alzheimers Dis. 23 (4) (2011) 567–598.
[25] M. Strong, A. Wolff, I. Wakayama, R. Garruto, Aluminum-induced chronic myelopathy in rabbits, Neurotoxicology 12 (1) (1991) 9–21.
[26] I. Wakayama, V. Nerurkar, R. Garruto, Immunocytochemical and ultrastructural evidence of dendritic degeneration in motor neurons of aluminum-intoxicated rabbits, Acta Neuropathol. 85 (2) (1993) 122–128.
[27] D. Crapper, S. Krishnan, A. Dalton, Brain aluminum distribution in Alzheimer's disease and experimental neurofibrillary degeneration, Science 180 (4085) (1973) 511–513.
[28] B. Ghetti, P. Gambetti, Comparative immunocytochemical characterization of neurofibrillary tangles in experimental maytansine and aluminum encephalopathies, Brain Res. 276 (2) (1983) 388–393.
[29] P. Zatta, Aluminum binds to the hyperphosphorylated tau in Alzheimer's disease: a hypothesis, Med. Hypotheses 44 (3) (1995) 169–172.
[30] J. Savory, C. Exley, W.F. Forbes, Y. Huang, J.G. Joshi, T. Kruck, D.R. Mclachlan, I. Wakayama, Can the controversy of the role of aluminum in Alzheimer's disease be resolved? What are the suggested approaches to this controversy and methodological issues to be considered? J. Toxicol. Env. Heal. A. 48 (6) (1996) 615–636.
[31] T. Mizoroki, S. Meshitsuka, S. Maeda, M. Murayama, N. Sahara, A. Takashima, Aluminum induces tau aggregation in vitro but not in vivo, J. Alzheimers Dis. 11 (4) (2007) 419–427.
[32] V.N. Uversky, J. Li, A.L. Fink, Metal-triggered structural transformations, aggregation, and fibrillation of human α-synuclein a possible molecular link between Parkinson's disease and heavy metal exposure, J. Biol. Chem. 276 (47) (2001) 44284–44296.
[33] Z.X. Xu, Q. Zhang, G.L. Ma, C.H. Chen, Y.M. He, L.H. Xu, Y. Zhang, G.R. Zhou, Z.H. Li, H.J. Yang, Influence of Aluminium and EGCG on fibrillation and aggregation of human islet amyloid polypeptide, J. Diabetes Res. (2016)https://doi.org/10.1155/2016/1867059.
[34] L. Su, C. Lu, P. Yan, N. Zhang, S. Cai, G. Zhang, X. Zhou, B. Li, The effect of aluminum ion on the aggregation of human islet amyloid polypeptide (11-28), Acta Bioch. Bioph. Sin. 49 (4) (2017) 355–360.
[35] S. Pal, S. Maity, S. Sardar, H. Parvej, N. Das, J. Chakraborty, U.C. Halder, Curcumin inhibits the Al (iii) and Zn (ii) induced amyloid fibrillation of β-lactoglobulin in vitro, RSC Adv. 6 (112) (2016) 111299–111307.
[36] P. Alam, S.K. Chaturvedi, M.K. Siddiqi, R.K. Rajpoot, M.R. Ajmal, M. Zaman, R.H. Khan, Vitamin k3 inhibits protein aggregation: implication in the treatment of amyloid diseases, Sci. Rep. 6 (2016), 26759.
[37] P. Alam, A.Z. Beg, M.K. Siddiqi, S.K. Chaturvedi, R.K. Rajpoot, M.R. Ajmal, M. Zaman, A.S. Abdelhameed, R.H. Khan, Ascorbic acid inhibits human insulin aggregation and protects against amyloid induced cytotoxicity, Arch. Biochem. Biophys. 621 (2017) 54–62.
[38] P. Alam, M.K. Siddiqi, S.K. Chaturvedi, M. Zaman, R.H. Khan, Vitamin B12 offers neuronal cell protection by inhibiting A beta-42 amyloid fibrillation, Int. J. Biol. Macromol. 99 (2017) 477–482.
[39] P. Alam, S. Borkokoty, M.K. Siddiqi, A. Ehtram, N. Majid, M. Uddin, R.H. Khan, DARK classics in chemical neuroscience: opium, a friend or foe, ACS Chem. Neurosci. 10 (1) (2018) 182–189.
[40] M.K. Siddiqi, P. Alam, S.K. Chaturvedi, M.V. Khan, S. Nusrat, S. Malik, R.H. Khan, Capreomycin inhibits the initiation of amyloid fibrillation and suppresses amyloid induced cell toxicity, BBA-Proteins Proteom 1866 (4) (2018) 549–557.
[41] M.K. Siddiqi, P. Alam, S. Malik, N. Majid, S.K. Chaturvedi, S. Rajan, M.R. Ajmal, M.V. Khan, V.N. Uversky, R.H. Khan, Stabilizing proteins to prevent conformational

changes required for amyloid fibril formation, J. Cell. Biochem. 120 (2) (2019) 2642–2656.
[42] B. Song, Q. Sun, H. Li, B. Ge, J.S. Pan, A.T.S. Wee, Y. Zhang, S. Huang, R. Zhou, X. Gao, Irreversible denaturation of proteins through aluminum-induced formation of backbone ring structures, Angew. Chem. Int. Ed. 126 (25) (2014) 6476–6481.
[43] Y. Zou, W. Hao, H. Li, Y. Gao, Y. Sun, G. Ma, New insight into amyloid fibril formation of hen egg white lysozyme using a two-step temperature-dependent FTIR approach, J. Phys. Chem. B 118 (33) (2014) 9834–9843.
[44] Y. Zou, Y. Li, W. Hao, X. Hu, G. Ma, Parallel β-sheet fibril and antiparallel β-sheet oligomer: new insights into amyloid formation of hen egg white lysozyme under heat and acidic condition from FTIR spectroscopy, J. Phys. Chem. B 117 (15) (2013) 4003–4013.
[45] V. Kocherbitov, J. Latynis, A. Misīūnas, J. Barauskas, G. Niaura, Hydration of lysozyme studied by Raman spectroscopy, J. Phys. Chem. B 117 (17) (2013) 4981–4992.
[46] L. Xing, K. Lin, X. Zhou, S. Liu, Y. Luo, Multistate mechanism of lysozyme denaturation through synchronous analysis of Raman spectra, J. Phys. Chem. B 120 (41) (2016) 10660–10667.
[47] R.A. Karaballi, S. Merchant, S.R. Power, C.L. Brosseau, Electrochemical surface-enhanced Raman spectroscopy (EC-SERS) study of the interaction between protein aggregates and biomimetic membranes, Phys. Chem. Chem. Phys. 20 (2018) 4513–4526.
[48] M. Tabatabaei, F.A. Caetano, F. Pashee, S.S. Ferguson, F. Lagugné-Labarthet, Tip-enhanced Raman spectroscopy of amyloid β at neuronal spines, Analyst 142 (23) (2017) 4415–4421.
[49] T. Deckert-Gaudig, V. Deckert, High resolution spectroscopy reveals fibrillation inhibition pathways of insulin, Sci. Rep. 6 (2016), 39622.
[50] D. Kurouski, R.P. Van Duyne, I.K. Lednev, Exploring the structure and formation mechanism of amyloid fibrils by Raman spectroscopy: a review, Analyst 140 (15) (2015) 4967–4980.
[51] V. Sereda, I.K. Lednev, Polarized Raman spectroscopy of aligned insulin fibrils, J. Raman Spectrosc. 45 (8) (2014) 665–671.
[52] L. Xing, W. Fan, N. Chen, M. N. Li, X. G. Zhou, S. L. Liu, Amyloid formation kinetics of hen egg white lysozyme under heat and acidic conditions revealed by Raman spectroscopy, (2019) DOI: https://doi.org/10.1002/jrs.5567.
[53] V. Shashilov, M. Xu, V.V. Ermolenkov, L. Fredriksen, I.K. Lednev, Probing a fibrillation nucleus directly by deep ultraviolet Raman spectroscopy, J. Am. Chem. Soc. 129 (22) (2007) 6972–6973.
[54] Y. Zhang, P.S. Cremer, The inverse and direct Hofmeister series for lysozyme, Proc. Natl. Acad. Sci. U. S. A. 106 (36) (2009) 15249–15253.
[55] R. Majumdar, P. Manikwar, J.M. Hickey, H.S. Samra, H.A. Sathish, S.M. Bishop, C.R. Middaugh, D.B. Volkin, D.D. Weis, Effects of salts from the Hofmeister series on the conformational stability, aggregation propensity, and local flexibility of an IgG1 monoclonal antibody, Biochemistry 52 (19) (2013) 3376–3389.
[56] D. Kurouski, T. Deckert-Gaudig, V. Deckert, I.K. Lednev, Surface characterization of insulin protofilaments and fibril polymorphs using tip-enhanced Raman spectroscopy (TERS), Biophys. J. 106 (1) (2014) 263–271.
[57] G. Ma, H. Zhang, J. Guo, X. Zeng, X. Hu, W. Hao, Assessment of the inhibitory effect of rifampicin on amyloid formation of hen egg white lysozyme: thioflavin T fluorescence assay versus FTIR difference spectroscopy, J. Spectrosc. (2014)https://doi.org/10.1155/2014/2858062014.
[58] M. Biancalana, S. Koide, Molecular mechanism of Thioflavin-T binding to amyloid fibrils, BBA-Proteins Proteom 1804 (7) (2010) 1405–1412.
[59] R. Sabaté, I. Lascu, S.J. Saupe, On the binding of Thioflavin-T to HET-s amyloid fibrils assembled at pH 2, J. Struct. Biol. 162 (3) (2008) 387–396.
[60] R. Khurana, C. Ionescu-Zanetti, M. Pope, J. Li, L. Nielson, M. Ramírez-Alvarado, L. Regan, A.L. Fink, S.A. Carter, A general model for amyloid fibril assembly based on morphological studies using atomic force microscopy, Biophys. J. 85 (2) (2003) 1135–1144.
[61] M. Biancalana, K. Makabe, A. Koide, S. Koide, Molecular mechanism of thioflavin-T binding to the surface of β-rich peptide self-assemblies, J. Mol. Biol. 385 (4) (2009) 1052–1063.
[62] M.R. Krebs, E.H. Bromley, A.M. Donald, The binding of thioflavin-T to amyloid fibrils: localisation and implications, J. Struct. Biol. 149 (1) (2005) 30–37.
[63] J.S. Richardson, D.C. Richardson, Natural β-sheet proteins use negative design to avoid edge-to-edge aggregation, Proc. Natl. Acad. Sci. U. S. A. 99 (5) (2002) 2754–2759.
[64] A. Herrero, P. Carmona, S. Cofrades, F. Jiménez-Colmenero, Raman spectroscopic determination of structural changes in meat batters upon soy protein addition and heat treatment, Food Res. Int. 41 (7) (2008) 765–772.
[65] A. Herrero, M. Cambero, J. Ordóñez, L. De la Hoz, P. Carmona, Raman spectroscopy study of the structural effect of microbial transglutaminase on meat systems and its relationship with textural characteristics, Food Chem. 109 (1) (2008) 25–32.
[66] N. Howell, E. Li-Chan, Elucidation of interactions of lysozyme with whey proteins by Raman spectroscopy, Int. J Food Sci. Tech. 31 (5) (1996) 439–451.
[67] T.G. Spiro, B.P. Gaber, Laser Raman scattering as a probe of protein structure, Annu. Rev. Biochem. 46 (1) (1977) 553–570.
[68] Z.Q. Wen, Raman spectroscopy of protein pharmaceuticals, J. Pharm. Sci. 96 (11) (2007) 2861–2878.
[69] I. Harada, T. Miura, H. Takeuchi, Origin of the doublet at 1360 and 1340 cm^{-1} in the Raman spectra of tryptophan and related compounds, Spectrochim. Acta A 42 (2–3) (1986) 307–312.
[70] M. Chen, R. Lord, R. Mendelsohn, Laser-excited Raman spectroscopy of biomolecules. V. Conformational changes associated with the chemical denaturation of lysozyme, J. Am. Chem. Soc. 96 (10) (1974) 3038–3042.
[71] S. Mangialardo, L. Gontrani, F. Leonelli, R. Caminiti, P. Postorino, Role of ionic liquids in protein refolding: native/fibrillar versus treated lysozyme, RSC Adv. 2 (32) (2012) 12329–12336.
[72] V.A. Shashilov, V. Sikirzhytski, L.A. Popova, I.K. Lednev, Quantitative methods for structural characterization of proteins based on deep UV resonance Raman spectroscopy, Methods 52 (1) (2010) 23–37.
[73] J. Kong, S. Yu, Fourier transform infrared spectroscopic analysis of protein secondary structures, Acta Biochim. Bioph. Sin. 39 (8) (2007) 549–559.
[74] A. Rygula, K. Majzner, K. Marzec, A. Kaczor, M. Pilarczyk, M. Baranska, Raman spectroscopy of proteins: a review, J. Raman Spectrosc. 44 (8) (2013) 1061–1076.
[75] M. Xu, V. Shashilov, I.K. Lednev, Probing the cross-β core structure of amyloid fibrils by hydrogen-deuterium exchange deep ultraviolet resonance Raman spectroscopy, J. Am. Chem. Soc. 129 (36) (2007) 11002–11003.
[76] V.A. Shashilov, M. Xu, V.V. Ermolenkov, I.K. Lednev, Latent variable analysis of Raman spectra for structural characterization of proteins, J. Quant. Spectrosc. Ra. 102 (1) (2006) 46–61.
[77] E. Frare, P. Polverino de Laureto, J. Zurdo, C.M. Dobson, A. Fontana, A highly amyloidogenic region of hen lysozyme, J. Mol. Biol. 340 (5) (2004) 1153–1165.
[78] I.W. Hamley, Peptide fibrillization, Angew. Chem. Int. Ed. 46 (43) (2007) 8128–8147.
[79] F. Chiti, C.M. Dobson, Protein misfolding, functional amyloid, and human disease, Annu. Rev. Biochem. 75 (2006) 333–366.
[80] I. Van Stokkum, H. Linsdell, J. Hadden, P. Haris, D. Chapman, M. Bloemendal, Temperature-induced changes in protein structures studied by Fourier transform infrared spectroscopy and global analysis, Biochemistry 34 (33) (1995) 10508–10518.
[81] A. Hédoux, J. Willart, R. Ionov, F. Affouard, Y. Guinet, L. Paccou, A. Lerbret, M. Descamps, Analysis of sugar bioprotective mechanisms on the thermal denaturation of lysozyme from Raman scattering and differential scanning calorimetry investigations, J. Phys. Chem. B 110 (45) (2006) 22886–22893.
[82] A. Hedoux, R. Ionov, J.F. Willart, A. Lerbret, F. Affouard, Y. Guinet, M. Descamps, D. Prevost, L. Paccou, F. Danede, Evidence of a two-stage thermal denaturation process in lysozyme: a Raman scattering and differential scanning calorimetry investigation, J. Chem. Phys. 124 (2006), 014703.
[83] M. Xu, V.A. Shashilov, V.V. Ermolenkov, L. Fredriksen, D. Zagorevski, I.K. Lednev, The first step of hen egg white lysozyme fibrillation, irreversible partial unfolding, is a two-state transition, Protein Sci. 16 (5) (2007) 815–832.
[84] R. Khurana, C. Coleman, C. Ionescu-Zanetti, S.A. Carter, V. Krishna, R.K. Grover, R. Roy, S. Singh, Mechanism of thioflavin T binding to amyloid fibrils, J. Struct. Biol. 151 (3) (2005) 229–238.
[85] J.A. Sweeney, S.A. Asher, Tryptophan UV resonance Raman excitation profiles, J. Phys. Chem. 94 (12) (1990) 4784–4791.
[86] R. Lord, N.-T. Yu, Laser-excited Raman spectroscopy of biomolecules: I. Native lysozyme and its constituent amino acids, J. Mol. Biol. 50 (2) (1970) 509–524.
[87] D.I. Ellis, D.P. Cowcher, L. Ashton, S. O'Hagan, R. Goodacre, Illuminating disease and enlightening biomedicine: Raman spectroscopy as a diagnostic tool, Analyst 138 (2013) 3871–3884.